Translational Oncology 14 (2021) 101186

Contents lists available at ScienceDirect

Translational Oncology

journal homepage: www.elsevier.com/locate/tranon

Original Research

TMEM180 contributes to SW480 human colorectal cancer cell proliferation through intra-cellular metabolic pathways

Takahiro Anzai [a], Shinji Saijou [a,b], Yoshitsugu Ohnuki [c], Hiroshi Kurosawa [c], Masahiro Yasunaga [a], Yasuhiro Matsumura [a,b,d,*]

[a] Division of Developmental Therapeutics, Exploratory Oncology Research & Clinical Trial Center, National Cancer Center, 6-5-1, Kashiwanoha, Kashiwa, Chiba, 277-8577, Japan
[b] Research division, RIN Institute Inc, 2-5-10, Shintomi, Chuo-Ku, Tokyo, 104-0041, Japan
[c] Faculty of Life and Environmental Sciences, Graduate Faculty of Interdisciplinary Research, University of Yamanashi, 4-4-37, Takeda, Kofu, Yamanashi 400-8510, Japan
[d] Department of Immune Medicine, National Cancer Center Research Institute, National Cancer Center, 5-1-1, Tsukiji, Chuo-Ku, Tokyo 104-0045, Japan

ARTICLE INFO

Keywords:
TMEM180
MFSD13A
Metabolomics
Nitric oxide synthase

ABSTRACT

TMEM180, a novel colon cancer–specific protein with a 12-transmembrane topology, is upregulated at low oxygen. Previously, we established a humanized monoclonal antibody against TMEM180 aimed at clinical trials. Prior to such trials, it is necessary to clarify the function of TMEM180 in cancer. To compare SW480 human colon cancer cells and their *TMEM180*-knockdown derivatives, we analyzed proliferation and oxygen consumption, and also performed phosphorylation proteomics, metabolomics, and next-generation sequencing (NGS). The preliminary results revealed that TMEM180 appeared to promote the growth of colon cancer but had almost no effect on oxygen consumption or expression of phosphorylated proteins. By contrast, glycolysis differed dramatically between SW480 and *TMEM180*-knockdown cells. The NGS analysis revealed that TMEM180 promotes enzyme expression in nitric oxide (NO) synthesis system, suggesting that it promotes glucose and glutamine metabolism, thereby contributing to cancer growth. Overall, the results of this study warrant further basic studies of TMEM180 molecule.

Introduction

Colorectal cancer (CRC) is the third leading cause of cancer death and has a high incidence and mortality worldwide [1]. Consequently, there is considerable incentive to identify new target molecules for the diagnosis and treatment of CRC. We previously identified a new membrane protein, TMEM180, that is highly expressed in CRC, and successfully developed the anti-TMEM180 monoclonal antibody (mAb) for future clinical use [2,3]. We reported that TMEM180 is upregulated under low-oxygen conditions and may play an important role in the uptake or metabolism of glutamine and arginine in cancer cell proliferation [2]. We also showed that *Tmem180*-knockout mice do not exhibit embryonic, neonatal, or postnatal lethality [2]. Recently, we found that TMEM180 has 12 transmembrane domains and that its N- and C-termini are exposed extracellularly [4]. TMEM180 was inferred to be a cation symporter [4], but its biological function in CRC cells remains unclear. In the present study, we focused on conducting various comparative studies between SW480 CRC wild cells and its gene knockdown cells in various methods including analysis of oxygen consumption, phosphorylated protein proteomics, next-generation sequencing, and metabolomics. Main purpose of this study is to find candidate molecules that are associated with the TMEM180 molecule in cancer growth and obtain a clue to the general role of TMEM180 in the growth of other CRC cells and clinical CRC.

Materials and Methods

Cells and cell cultures

SW480 cells were purchased from American Type Culture Collection. Cells were cultured in DMEM low-glucose medium (Wako) supplemented with 10% FBS (Thermo Fisher Scientific) and 1% penicillin–streptomycin–amphotericin B suspension (Wako) at 37°C under a 5% CO_2 atmosphere. Clones of SW480 cells harboring stable knockdown

* Corresponding author.
E-mail address: yhmatsum@ncc.go.jp (Y. Matsumura).

https://doi.org/10.1016/j.tranon.2021.101186
Received 10 May 2021; Received in revised form 19 July 2021; Accepted 21 July 2021
1936-5233/© 2021 The Authors. Published by Elsevier Inc. This is an open access article under the CC BY license (http://creativecommons.org/licenses/by/4.0/).

of *TMEM180* were established as described previously [2]. Lentiviral transduction particles were used to generate stable knockdown cells (Sigma-Aldrich, MISSION TRC clones TRCN0000243137 for *TMEM180* knockdown and SHC005V for *eGFP* knockdown; the latter was used as the Mock control).

Quantitative real-time RT-PCR

To measure the level of *TMEM180* mRNA in stable knockdown cells, quantitative real-time RT-PCR was performed as described previously [2]. The relative expression of *TMEM180* was normalized against expression of *GAPDH*. Statistical analysis of the data was performed using the Mann-Whitney U test for non-parametric data.

Cell proliferation assay

For the CCK-8 assay, SW480 cells were seeded at 250 cells per well in 200 μL culture medium in 96-well cell culture plates (Corning) on day 0. After culturing for 2, 4, 6, or 7 days at 37°C, 5% CO_2, cell proliferation was measured using the Cell-Counting Kit 8 (Dojindo, CCK-8). CCK-8 solution was added (10 μL per well), and the plate was incubated for 3 h. Absorbance of each well was measured at 450 nm. For the anchor-independent cell proliferation assay, SW480 cells were seeded at 125 cells per well in 200 μL culture medium in round-bottom Ultra Low Attachment (ULA) 96-well plates (Corning). The ULA plates were centrifuged at 100 × g for 3 min, and the cells were cultured at 37°C under 5% CO_2 with shaking at 80 rpm. Images were acquired on a Keyence Microscope BZX-700 (Keyence) on day 0 (12 h), day 2, day 4, day 6, and day7 after cells were seeded. Statistical analysis of the data was performed using the Mann-Whitney U test for non-parametric data.

Measurement of respiratory rate

A respiratory rate measurement system using a spinner flask was constructed as described in Fig .2a. The spinner flask was filled with 60 mL of DMEM low-glucose medium and incubated at 35°C under a 4% CO_2 atmosphere with gentle stirring at 80 rpm. Cell suspension (5 mL of 7–8 × 10^7 cells) was inoculated, and dissolved oxygen concentration in the spinner flask was measured with an oxygen probe (DKK Co., DOL-10). First, the volumetric oxygen transfer coefficient k_La was determined as follows. Dissolved oxygen in the medium was purged by nitrogen substitution. After the dissolved oxygen concentration (C) was lowered to near zero, the medium was re-oxygenated using the gas atmosphere in the incubator, described above. Dissolved oxygen concentration was recorded as a function of time. The slope of the curve, the derivative $\frac{dC}{dt}$, corresponds to the oxygen transfer rate, and is expressed by equation (a).

$$\frac{dC}{dt} = k_La(C^* - C)\ (a)$$

C^*: saturated dissolved oxygen concentration [mg-O_2·L^{-1}]
C: dissolved oxygen concentration [mg-O_2·L^{-1}]
k_La: oxygen transfer capacity coefficient [min^{-1}]
t: time [min]

Integration of equation (a) under the initial conditions $t = 0$ and $C = C_0$ yields equation (b).

$$ln\frac{(C^* - C)}{(C^* - C_0)} = -k_La{\cdot}t\ (b)$$

Based on equation (b), k_La was calculated to be 0.064 [min^{-1}] from the slope of a straight line on a semi-log plot. For the cell culture system, a term for respiration rate (r_{o2}) is added to the equation (a).

$$\frac{dC}{dt} = k_La(C^* - C) - r_{O2}\ (c)$$

$$r_{O2} = Q_{O2}{\cdot}X\ (d)$$

r_{o2}: respiration rate [mg-O_2·L^{-1}·min^{-1}]
Q_{O2}: specific respiration rate [mg-O_2·$cells^{-1}$·min^{-1}]
X: cell concentration in the measurement system [cells·L^{-1}]

At steady state, the oxygen supply rate (k_La (C*-C)) and the respiration rate (r_{o2}) are balanced, and the dissolved oxygen concentration (C) reaches equilibrium, i.e., $\frac{dC}{dt} = 0$. Therefore, equation (e) can be obtained from equation (c).

$$r_{O2} = k_La(C^* - C)(e)$$

Here, the dissolved oxygen concentration in equilibrium is indicated as C_E in notation. Specific respiratory rate (Q_{O2}) was calculated by substituting the value of C_E into equation (f).

$$Q_{o2} = \frac{r_{o2}}{X} = \frac{k_La(C^* - C_E)}{X}\ (f)$$

C_E: dissolved oxygen concentration at steady state [mg-O_2·L^{-1}]

Preparation of phosphoprotein-enriched extracts

Cultured cells were washed three times with PBS, and pellets were harvested in sample buffer containing 4% SDS, 125 mM Tris-HCl (pH 6.8), and 0.04% bromophenol blue. Protein solutions were boiled 95°C for 5 min and stored at -20°C. Samples were dissolved in a sample lysis solution containing 7 M urea, 2 M thiourea, 4% (w/v) 3-[(3-cholamidopropyl)dimethyammonio]-1-propanesulfonate (CHAPS), 1% (w/v) dithiothreitol (DTT), 2% (v/v) Pharmalyte, and 1 mM benzamidine, and homogenized using a PowerGen125 motor-driven homogenizer (Thermo Fisher Scientific). Total proteins were extracted for 15 min at room temperature with vortexing, and the extract was centrifuged at 12,000 × g for 20 min at 25°C. The PhosPro Phosphoprotein enrichment kit (Genomine) was used to isolate phosphoproteins from total protein extracts. Subsequently, the sample was mixed with 750 μL of delipidation solution (methanol:chloroform = 600:150), vortexed vigorously for 5 min, and centrifuged at 15,000 × g for 10 min to promote phase separation. The middle phase containing the protein disk was recovered, and the upper and lower phases were discarded. The protein disk was washed twice in ~1 mL methanol. The protein pellet was completely air-dried or dried in an oven and dissolved in a buffer for 2D electrophoresis.

2D. electrophoresis

IPG strips (Genomine) were reswelled for 12–16 h at room temperature in a solution containing 7 M urea, 2 M thiourea, 2% CHAPS, 1% DTT, and 1% Pharmalyte. Isoelectric focusing was performed using 800 μg protein sample per strip on a MultiPhor II system (Amersham Biosciences) at 20°C. The voltage was sequentially increased from 0.15 to 3.5 kV over 3 h to allow entry of the sample, followed by maintenance at 3.5 kV over 9 h, with focusing completed after 96 kV-h. IPG strips were incubated for 10 min in equilibration buffer (50 mM Tris-HCl, pH 6.8 containing 6 M urea, 2% SDS, and 30% glycerol), first with 1% DTT and second with 2.5% iodoacetamide. Equilibrated strips were loaded onto SDS-PAGE gels (10 cm × 12 cm, 10–16%), and SDS-PAGE was performed on a Hoefer DALT 2D system (Amersham Biosciences) at 20°C for 1.7 kV-h. Gels were fixed with a solution containing 40% (v/v) ethanol and 10% (v/v) acetic acid for 1 h, and then stirred three times for 30 min in a rehydration solution (5% (v/v) ethanol and 5% (v/v) acetic acid in distilled water. Phospho-proteins were visualized using ProQ Diamond phospho-protein gel stain (Invitrogen) for 2 h, and then washed with ProQ Diamond phospho-protein destaining solution (Invitrogen) for 60 min. Gel images were acquired using DIVERSITY (Syngene). The gels were washed with distilled water three times and stained with Coomassie Brilliant Blue G-250 (Invitrogen). Images were acquired on a Duoscan T1200 (Agfa). Intensities of individual protein

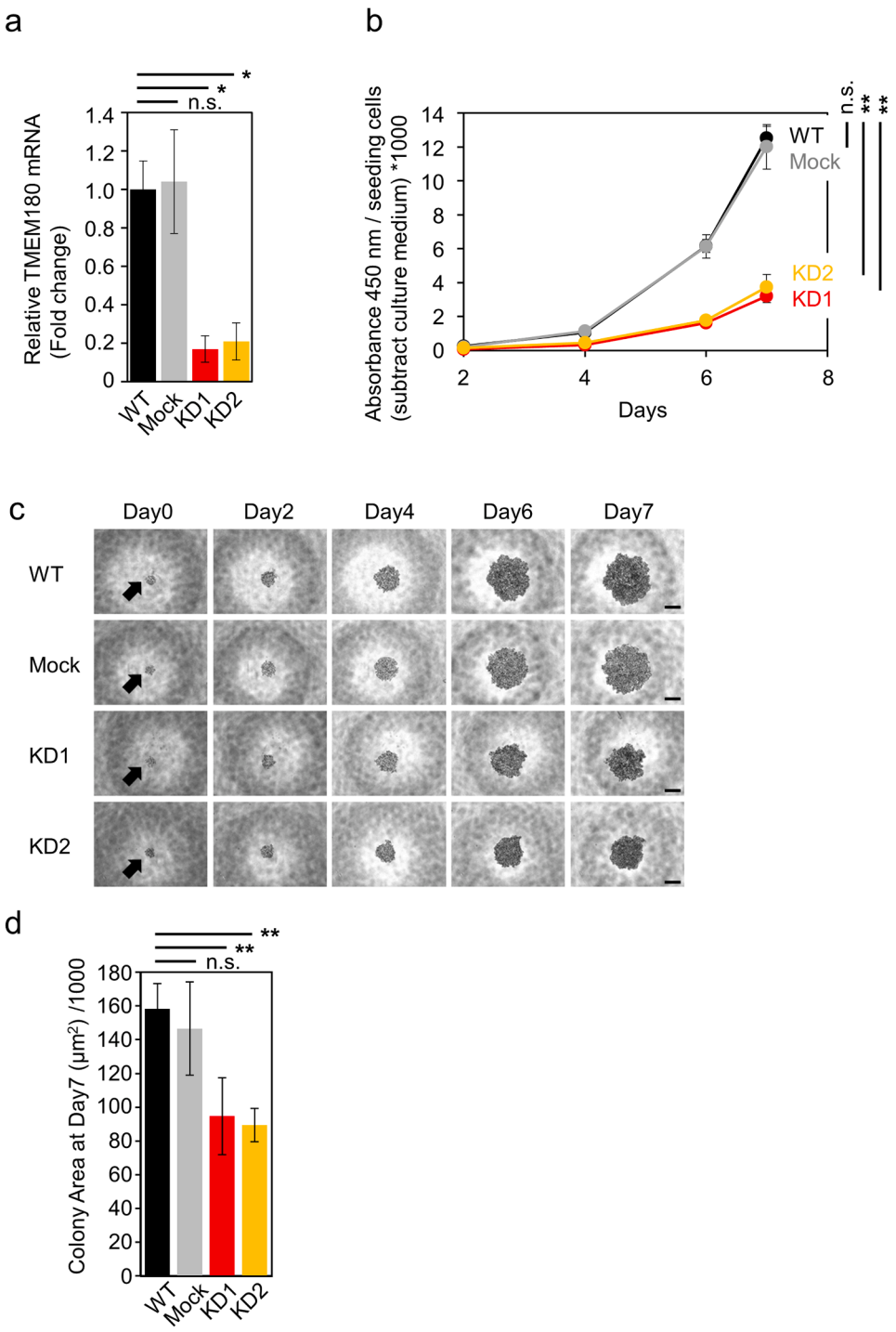

Fig 1. *TMEM180* knockdown suppresses SW480 cell proliferation

(a). Relative expression of *TMEM180* in SW480 (WT), SW480 expressing control shRNA (Mock), and SW480 expressing *TMEM180*-specific shRNA (KD1 and KD2) was measured by qRT-PCR. *$p < 0.05$, n.s. = not significant. Bars = SD.

(b). Effect of *TMEM180* knockdown on cell proliferation. CCK-8 assays indicated that *TMEM180* knockdown suppressed cell proliferation. Absorbance at 450 nm was multiplied by 1000 after subtraction of background value (culture medium without cells), and then normalized against cell number. Statistical analysis was performed using the value from Day 7. ** $p < 0.01$, n.s. = not significant. Bars = SD.

(c). Typical microscope images of SW480 WT, Mock, KD1 and KD2 cells taken on Day 0 (12 h after seeding cells), Day 2, Day 4, Day 6, and Day7. Scale bars: 200 μm.

(D). Cell colony area on Day 7, calculated using ImageJ1.52 from six independent wells. **$p <$ 0.01, Bars $p <$ SD.

spots were normalized against the total intensities of all valid spots. Analysis was performed using the PDQuest 2D analysis software (Bio-Rad). Protein spots that exhibited a significant (≥2-fold) change in expression between WT and KD were selected for further analysis.

PMF analysis

Selected protein spots were excised from the gel and enzymatically digested in-gel essentially as previously described[5] using trypsin (Promega). Gel pieces were washed with 50% acetonitrile to remove SDS, salt, and stain; dried to remove solvent; and then rehydrated with trypsin and incubated for 12 h at 37°C. The proteolytic reaction was terminated by addition of 5 μL 0.5% trifluoroacetic acid. Tryptic peptides were recovered by combining the aqueous phase from several extractions of the gel pieces with 50% aqueous acetonitrile. After concentration, the peptide mixture was desalted using C18ZipTips (Millipore), and peptides were eluted in 1–5 μL of acetonitrile. An aliquot of this solution was mixed with an equal volume of saturated solution of α-cyano-4-hydroxycinnamic acid in 50% aqueous acetonitrile / 0.1% TFA, and 1 μL of the mixture was spotted onto a target plate. Proteins were subjected to MALDI-TOF analysis (Bruker Daltonics, Microflex LRF 20) as described previously[6]. The search program MASCOT, developed by Matrix Science, was used for protein identification by peptide mass fingerprinting.

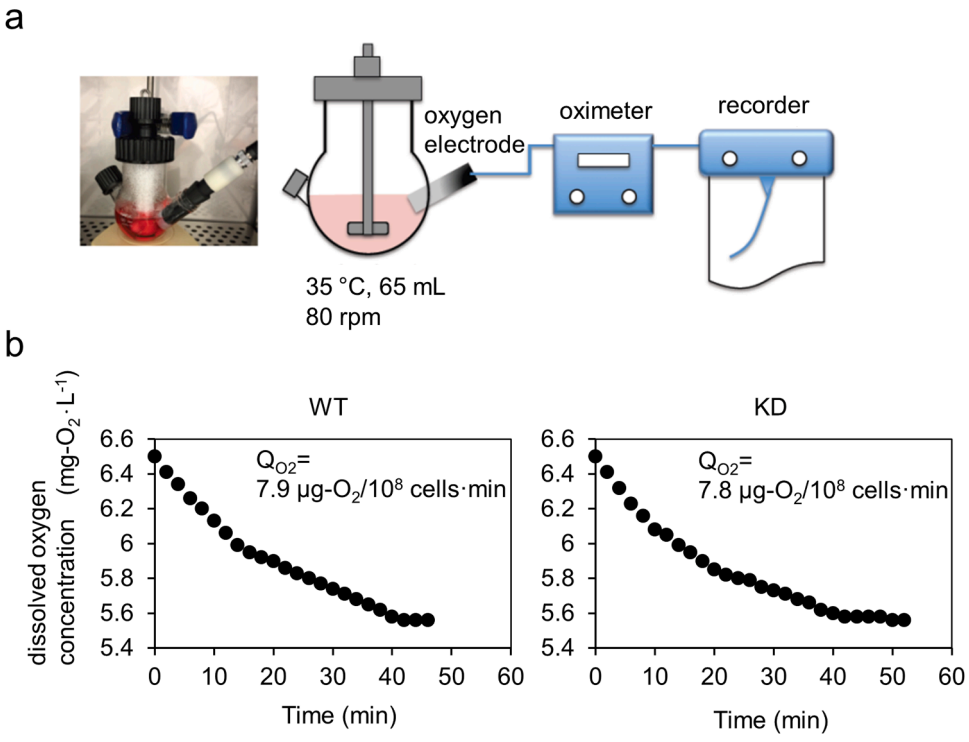

Fig. 2. Respiration rate of SW480 cells
(a). Oxygen concentration profiles in spinner flasks inoculated with cells.
(b). Cell respiration data plot and respiration rate of WT (left) and KD (right) cells.

Metabolite extraction

Cells were grown to a density of 1–5 × 10^6 cells per 10 cm dish, washed three times with PBS, and cultured in DMEM low-glucose medium without FBS. After 3 h, culture medium was removed from the dish, and the cells were washed twice in 5% mannitol solution, first with 10 mL and next with 2 mL. Metabolites were extracted from 2.7–3.0 × 10^6 cells with 800 μL methanol and 550 μL Milli-Q water containing Internal Standard Solution (Human Metabolome Technologies [HMT]) for CE-MS, and with 1300 μL ethanol containing Internal Standard Solution for LC-MS. Extracts for CE-MS were transferred into a microfuge tube and centrifuged at 2,300 × g at 4°C for 5 min. To remove proteins, the extracts were centrifugally filtered through a 5 kDa cutoff filter (Millipore) at 9,100 × g at 4°C for 2 h. Extracts were stored at -80°C until analysis. Before measurement, extracts for CE-MS were centrifugally concentrated and resuspended in 50 μL of Milli-Q water for measurement. Extracts for LC-MS were mixed with 1,000 μL Milli-Q water and sonicated for 5 min while cooling on ice, and the supernatant was collected by centrifugation (4,400 × g, 4°C, 5 min). It was dissolved in 200 μL of 50% aqueous isopropanol solution (v/v) and used for the measurement.

Metabolomic analysis

Targeted quantitative analysis of metabolites was performed by HMT using capillary electrophoresis time-of-flight mass spectrometry (CE-TOF/MS), capillary electrophoresis triple quadrupole mass spectrometry (CE-QqQMS), and liquid chromatography time-of-flight mass spectrometry (LC-TOF/MS). Analytic methods were described previously [7]. CE-TOFMS measurement was performed on an Agilent CE-TOFMS system, CE-MS/MS measurement was performed on an Agilent CE system with Agilent 6460 TripleQuad LC/MS, and LC-TOFMS measurement was performed using an Agilent 1200 series RRLC system SL with Agilent LC/MSD TOF (all machines: Agilent Technologies). Peaks detected by CE-TOF/MS and LC-TOF/MS were extracted using MasterHands ver2.17.1.11 (Keio University), and peaks detected by CE-MS/MS were extracted using MassHunter Quantitative Analysis B.06.00 (Agilent Technologies). Migration time (for CE-MS), retention time (for LC-MS), *m/z*, and peak area were obtained from the software. The peaks were annotated according to the HMT metabolite database based on their *m/z* values with the Migration times or retention times. The obtained relative area value was converted into an absolute quantitative value using a standard substance. The peak area value corrected by the internal standard substance was used for quantitative conversion. A calibration curve consisting of three points was created for each metabolite, and the concentration was calculated. Hierarchical Cluster Analysis (HCA) and Principal Component Analysis (PCA) were performed by HMT using in-house analysis software developed by the company. Statistical analysis of the data was performed using the Mann-Whitney U test for non-parametric data.

RNA-seq and enrichment analysis

Total RNA was extracted using the RNeasy Mini kit (Qiagen). RNA quality checking, library preparation, and sequencing on the HiSeq 4000 platform (Illumina) were performed by Eurofins Genomics. All samples had an RNA Integrity Number (RIN) > 9.7. Trimmomatic [8] ver0.36 was used to remove adaptor sequences and low-quality reads from the sequencing data. BWA [9] ver0.7.17 was used to map reads onto the human reference genome assembly GRCh38.p12. Count files produced by featureCounts [10] were normalized and statistically analyzed by the edgeR package using TCC-GUI [11]. Differentially expressed genes (DEGs) compared with each group were identified with a q value < 0.1. Enrichment analysis was performed on upregulated or downregulated DEGs using Metascape [12]. Statistical analysis of the data was performed using the Mann-Whitney U test for non-parametric data.

a

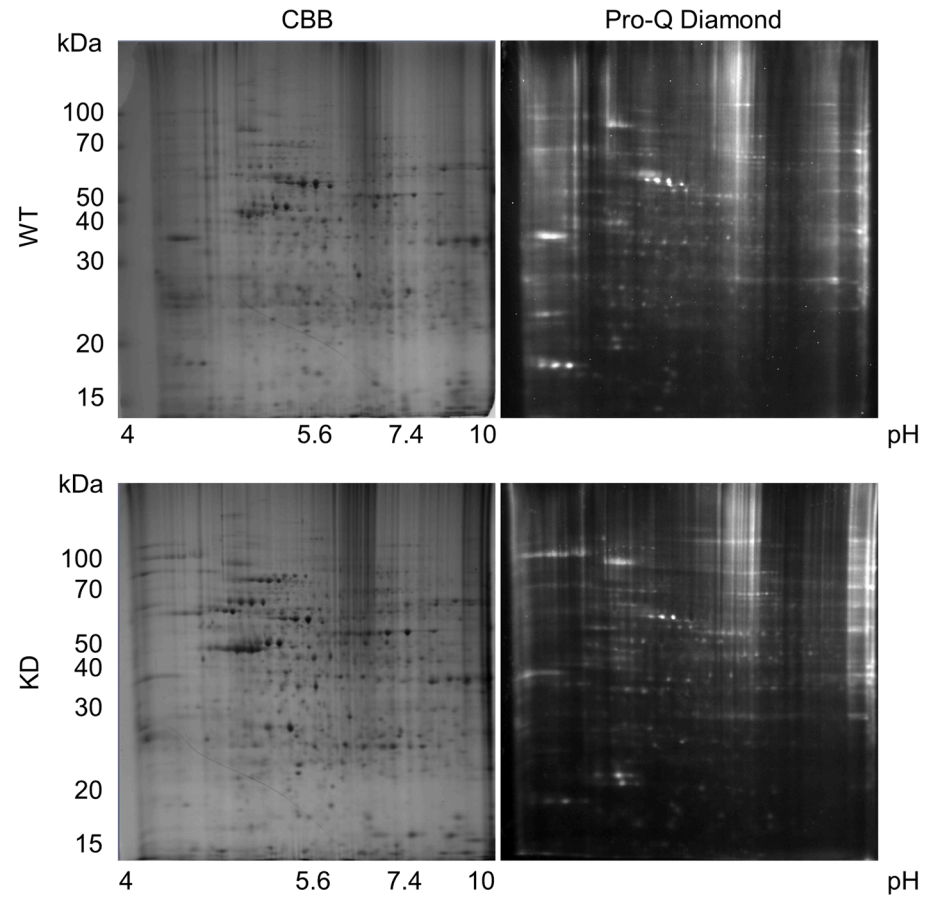

Fig. 3. Phospho-protein patterns of SW480 cells, monitored by 2D gel electro-phoresis
(a). 2D gel images from one of three independent experiments are shown. Upper panels represent WT cells, and lower panels represent KD cells. Left panels show Coomassie Brilliant Blue (CBB) staining, and right panels show ProQ Diamond staining. Y-axes indicate apparent molecular mass (kDa), and X-axes indicate pH.
(b). Results of differential spot analysis. MW is the predicted molecular weight of the spot, and pI is the predicted isoelectric point of the spot.

b

Spot	1		2	
MW	24.08		51.27	
pI	5.17		6.91	
	Spot intensity In CBB	Spot intensity in Pro-Q	Spot intensity In CBB	Spot intensity in Pro-Q
WT-1	26.3	217	962.6	263.2
WT-2	167.6	151.5	1033.1	241.3
WT-3	183.8	412.4	1513.2	377.7
KD-1	-	-	1664.8	1093.2
KD-2	-	-	1893.4	984.1
KD-3	-	-	1663.8	1050.9
Defenition	epididymis luminal protein 176		alpha-enolase	

Results

TMEM180 gene knockdown suppress cell proliferation of SW480 colon cancer cells

To explore molecular function of TMEM180 in cancer cells, we established *TMEM180*-knockdown SW480 cell clones using shRNA (Fig. 1a). To evaluate effects of *TMEM180* gene knockdown, we performed cell proliferation assay of SW480 cells. Cell proliferation was significantly lower in *TMEM180*-knockdown cell clones (KD1 and KD2) than in the parental cell line (WT) or cells expressing a control shRNA (Mock) (Fig. 1b). Next, we compared anchoring independent cell proliferation between WT, Mock and KD cells. Anchorage-independent cell proliferation was also significantly suppressed in *TMEM180*-knockdown cell clones (KD1 and KD2) relative to WT and Mock (Fig. 1c, d). We also conclude that there is no difference between WT and Mock in cell proliferation. In our recent publication, we found that tumorigenesis was also suppressed by TMEM180 gene knockdown confirmed by colony-forming activity in soft agar (*in vitro*) and tumor-initiating activity in mice (*in vivo*) [3].

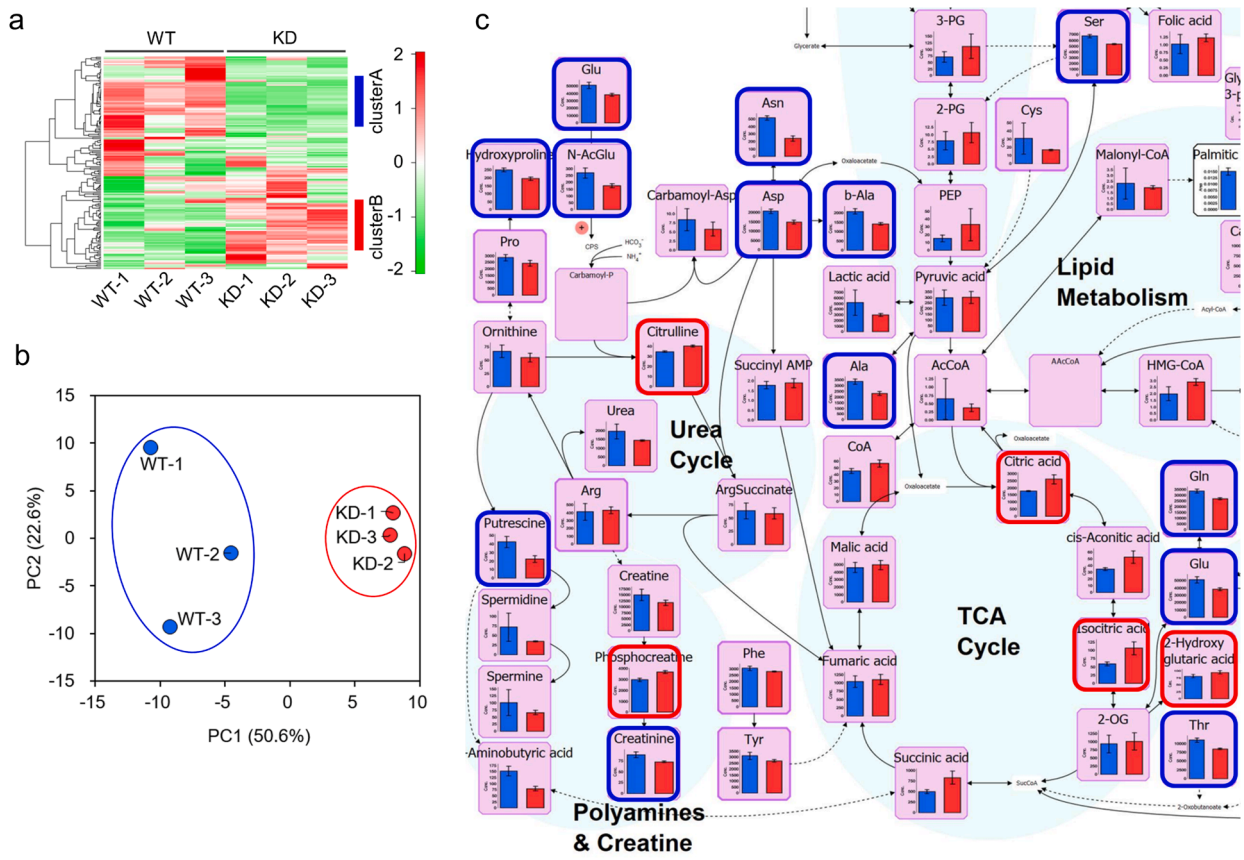

Fig 4. Metabolomics analysis of SW480 cells
(a). Heat map representation of meta-bolome profiles analyzed by hierarchical clustering analysis. Cluster A (blue line) and cluster B (red line) are shown on the right edge of the figure.
(b). Score plot of principal component 1 (PC1) versus principal component 2 (PC2) from the principal component analysis (PCA). Clustering of WT samples (blue circle) and KD samples (red circle) is shown.
(c). Graphical representation of metabolites mapped to known pathways around TCA cycle. Bar graphs represent the amounts of metabolites (exceptions: Palmitic acid and cholesterol are relative values) in WT (blue) and KD (red) cell samples. Metabolites that were significantly more abundant in WT are highlighted with blue squares, and those that were more abundant in KD are highlighted with red squares.

TMEM180 gene knockdown does not contribute to SW480 cell respiration rate

Oxygen concentration profiles in the spinner flasks inoculated with SW480 WT and SW480 KD cells are shown in Fig. 2a. Specific respiration rate (Q_{O2}), oxygen consumption rate per unit cell, was calculated based on the equation (f) described in the part of Materials and Methods. In this equation, C_E means the dissolved oxygen concentration at a steady state, in which the oxygen supply rate and the respiration rate are balanced. There is no significant difference in Q_{O2} between SW480 WT and SW480 KD cells (Fig. 2b). The results suggest that *TMEM180* gene knockdown does not have an effect on cell respiration. It is supposed that TMEM180 is not involved in the function of oxygen uptake in cells or mitochondria. The correlation between cell proliferation and oxygen consumption is well known in cancer cells [13]. In this study, it was found that cell proliferation was promoted in SW480 WT cells. Moreover, SW480 WT cells formed spherical cell aggregates that were larger in size than SW480 KD cells. The increase in cell number or in size of cell aggregate will increase the overall oxygen consumption, but it may not be directly linked to the oxygen consumption rate per unit cell (Q_{O2}). These observations suggest that TMEM180 is not involved in oxygen uptake in cells or mitochondria.

TMEM180 gene knockdown has little effect on phospho-protein expression

To investigate changes in phosphorylation proteins associated with *TMEM180* gene knockdown, we performed phospho-proteomics analysis between WT and KD cells. We identified enriched phosphoproteins by 2D gel electrophoresis followed by staining with CBB and ProQ Diamond (Fig. 3a). Only two protein spots differed in intensity between WT and KD cells (Fig. 3a,b). By searching the database using the Mascot server, we identified spot 1 as epididymis luminal protein 176 and spot 2 as alpha-enolase (Fig. 3b). Based on the UniProtKB [14] annotation, epididymis luminal protein 176 (UniProtKB: V9HVZ7) has an unknown function, but may belong to the actin family. The other protein, alpha-enolase (ENO1) (UniProtKB: P06733), is a key enzyme in the glycolytic pathway [15], and its expression is correlated with cancer progression or metastasis [16,17]. It is not known whether phosphorylation of ENO1 is related to cancer. These results indicate that TMEM180 has a minimal effect on phosphoprotein expression.

TMEM180 gene knockdown cause variation in metabolites around glycolysis

To investigate the metabolite profile changes associated with *TMEM180* gene knockdown, we performed capillary electrophoresis time of flight mass spectrometry (CE-TOF/MS), capillary electrophoresis-triple quadrupole mass spectrometry (CE-QqQMS) and liquid chromatograph time of flight mass spectrometry (LC-TOF/MS). In this analysis, we detected a total of 161 metabolites (CE-MS: 44 and 57 in cation and anion mode, respectively; LC-MS: 46 and 14 metabolites in positive and negative mode, respectively). The heat map in Fig. 4a

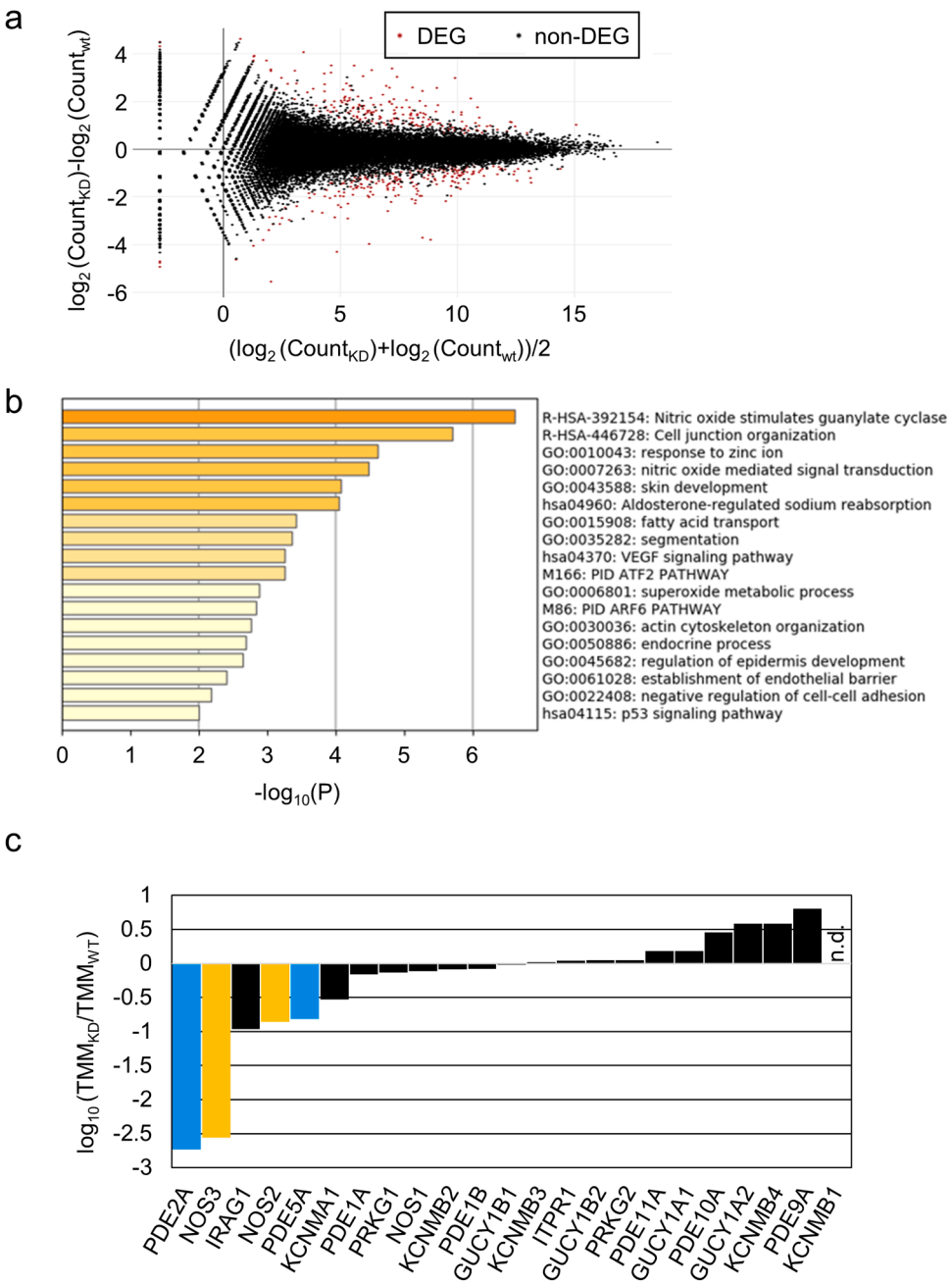

Fig 5. RNA-seq analysis of SW480 cells
(a). MA plot comparing WT and KD cells. Genes colored in red were selected as DEGs using an FDR q-value threshold of 0.1.
(b). Function enrichment analysis of DEG correlated with *TMEM180* KD from between WT and KD cell samples.
(c). Relative expression of 23 genes involved in nitric oxide stimulates Guanylate Cyclase pathway. *PDE2A* and *PDE5A* shows in cyan, *NOS2* and *NOS3* shows in yellow. n.d.= no data.

represents two major clusters. In cluster A, several amino acids and acylcarnitine-related metabolites were present at higher levels in WT cells than in KD cells. In cluster B, levels of phospholipid- and glycolysis-related metabolites were elevated in KD cells relative to WT cells (Supplementary Table 1). The score plot of the principal component analysis (PCA) revealed a clear separation between WT and KD along the first principal component (PC1) axis (Fig. 4b). Glycolytic metabolites and lysophospholipids were included among the top 30 metabolites with positive values of the principal component score (Supplementary Table 2), and amino acids and acylcarnitine were included in the top 30 metabolites with negative values (Supplementary Table 3). The detected metabolites were mapped to known pathways of glycolysis and amino acid metabolism (Fig. 4c and Supplementary Fig. 1). Related metabolites upstream of glycolysis were more abundant in KD cells (Fig. 4c and Supplementary Fig. 1, highlighted in red square). However, there was no difference in the amount of pyruvic acid or lactate. In addition, levels of amino acids such as Asn, Asp, Gln, Glu, and Ser that flow into the glycolysis pathway were significantly higher in WT cells Fig. 4c and Supplementary Fig. 1, highlighted in blue square). Based on these results, knockdown of *TMEM180* appeared to affect glycolysis and amino acid metabolism.

TMEM180 gene knockdown cause down-regulation of nitric oxide synthase and glutaminase

In RNA-seq analysis, the MA plot revealed that 165 genes were downregulated, and 160 genes were upregulated, with q-value < 1.0 (Fig. 5a). In biological enrichment analysis of the downregulated genes using Metascape [12], nitric oxide (NO) stimulation of guanylate cyclase (Reactome [18] Gene Sets) was top-ranked (Fig. 5b). In this pathway, nitric oxide synthase (NOS) produces NO, which oxidizes a guanidine nitrogen of L-arginine. NO activates soluble guanylate cyclase (sGC) and increases the conversion of cyclic guanylate monophosphate (cGMP) from guanosine 5′-triphosphate (GTP). Phosphodiesterases (PDE)

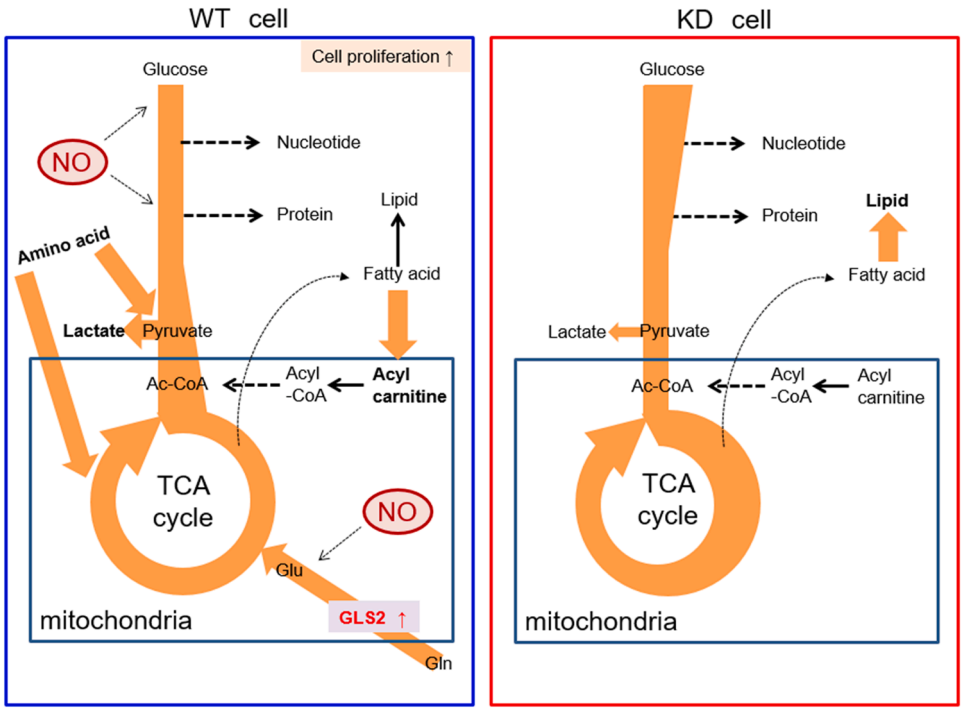

Fig 6. Schematic model of metabolic flux in SW480 cells and *TMEM180* KD derivatives
Metabolic fluxes revealed in this study are shown. Arrow direction indicates metabolite flux. Bold type indicates a large quantity of metabolites. Nitric oxides are shown as red circle, and Glutaminase GLS2 is shown in red font.

degrade cGMP by hydrolyzing cGMP into 5′-GMP (Supplementary Fig. 2a). This pathway contains 23 proteins (Supplementary Fig. 2b).

NO is an essential molecule involved in several pathophysiological processes in mammals [19]. Three isoforms of NOS have been identified: neuronal (nNOS or NOS1), inducible (iNOS or NOS2), and endothelial (eNOS or NOS3) [19]. We found that expression of *NOS2* and *NOS3* was higher in WT cells than in KD cells (Supplementary Fig. 2c).. PDE is a key enzyme that hydrolyzes cGMP and cAMP, and 11 families are known [20]. PDEs can be classified into three types according to their specificity to cyclic nucleotides. PDE4, PDE7, and PDE8 are specific to cAMP, whereas PDE5, PDE6, and PDE9 specific to cGMP. The other PDEs (PDE1, PDE2, PDE3, PDE10, and PDE11) hydrolyze both cAMP and cGMP [21]. We found that expression of *PDE2A* and *PDE5A* was higher in WT cells than in KD cells (Supplementary Fig. 2c).

We next analyzed public TCGA data (https://www.cancer.gov/tcga) to search for genes that correlate with *TMEM180* expression. Correlation analysis between normal and primary tumors was performed using UALCAN [22]. *GLS2* was the only relevant metabolic enzyme out of the top 10 positively correlated genes (Supplementary Fig. 3a). The correlation between *TMEM180* (x-axis) and *GLS2* (y-axis) is visualized as Supplementary Fig. 3b. We confirmed that expression of *GLS2* was higher in WT cells than in KD cells (Supplementary Fig. 3c). We previously reported that *TMEM180*-knockdown cells could not grow in serum-free medium without glutamine and arginine [2]. Thus, TMEM180 may play an important role in the uptake or metabolism of glutamine and arginine during tumor growth and proliferation [2]. Based on these findings, we hypothesized that TMEM180 is related to both NO-related metabolism and glutamine metabolism.

Discussion

TMEM180 gene knockdown in SW480 CRC cells was demonstrated at both protein and mRNA levels. Decreased proliferation of SW480KD indicated that TMEM180 is involved in the growth of human CRC cell line SW480 (Fig. 1). To investigate the mechanisms involved in proliferation, we compared respiratory rate, phosphorylation signals, and metabolites between SW480 WT and its *TMEM180*-knockdown derivative. The results revealed that TMEM180 does not contribute to cellular respiration rate (Fig. 2) and has little effect on phosphoprotein expression (Fig. 3). On the other hand, TMEM180 caused variation in metabolites related to glycolysis (Fig. 4). RNA-seq analysis revealed that *NOS2, NOS3, PDE2A, PDE5A* and *GLS2* genes were downregulated in *TMEM180* KD cells (Supplementary Fig. 2c and 3c). NO may influence glucose and glutamine utilization in tumor cells directly or through the activation of oncogenic pathways [19]. Glutaminase catalyzes the conversion of glutamine into glutamate. There are two subtypes of glutaminase: GLS (kidney-type) and GLS2 (liver-type) [23]. Elevated expression of GLS has been observed in several types of cancer [24]. In CRC, high expression of GLS is correlated with poor prognosis [25]. High expression of GLS2 is positively correlated and reduced overall survival in patients with colon, blood, ovarian, and thymoma cancer [26]. By contrast, overexpression of GLS2 acts in an anti-oncogenic manner in liver and brain cancer [27,28]. Hence, we analyzed TCGA data from CRC using GEPIA2 [29]. The results revealed that expression of neither *GLS* nor *GLS2* was associated with poor prognosis (Supplementary Fig. 4a,b). In our RNA-seq data, expression of *GLS* was unchanged (Supplementary Fig. 4c). Thus, the relationship between expression of GLS2 and cancer proliferation in patients remains controversial.

In *TMEM180* KD cells, the upstream of glycolytic pathway is enhanced, but there was no change in the amount of pyruvic acid, and the amount of lactate was higher in WT cells. Activation of glycolysis by NO, activation of the glutamine pathway by high expression of GLS2, and amino acid uptake were observed in SW480 WT cells, suggesting that proliferation was promoted in SW480 WT cells with high TMEM180 expression (Fig. 6). Recently, Mei et al. reported that siRNA-mediated knockdown of *MFSD13A/TMEM180* promotes proliferation of pancreatic cancer cell lines [30]. On the other hand, we showed that shRNA-mediated knockdown of *TMEM180* suppressed proliferation of SW480 cells (Fig. 1). Thus, the role of TMEM180 in proliferation may differ depending on the type of cancer. Further studies in different types of cancer are needed to resolve this potential contradiction.

In conclusion, we showed that TMEM180 contributes to the growth

of SW480 human CRC by altering metabolism, rather than signal transduction or mitochondrial function. In order to generalize this finding in CRC or other cancers, it is important to confirm the data with various cells or clinical specimens. In future work, it will also be important to identify the substrate that is transported by coupling with cations and to clarify the involvement of TMEM180 in NO-related metabolism, glutamine metabolism and the tumor growth. We acknowledge that the present findings are insufficient to convey the function and properties of the TMEM180 molecule. We, however, anticipate that these findings will help elucidate more precisely the role of TMEM180 in cancer cells.

CRediT authorship contribution statement

Takahiro Anzai: Methodology, Investigation, Visualization, Writing – original draft, Writing – review & editing, Funding acquisition. **Shinji Saijou:** Investigation. **Yoshitsugu Ohnuki:** Methodology, Investigation. **Hiroshi Kurosawa:** Methodology, Investigation. **Masahiro Yasunaga:** Methodology, Funding acquisition. **Yasuhiro Matsumura:** Conceptualization, Methodology, Writing – review & editing, Supervision, Funding acquisition.

Declaration of Competing Interest

Yasuhiro Matsumura is co-founder, shareholder, and Board Member of RIN Institute, Inc. Shinji Saijou is an employee of RIN Institute, Inc. Masahiro Yasunaga is a shareholder of RIN Institute, Inc. The other authors declare no competing interests.

Statistical analysis

All statistical analyses were performed with EZR version 1.42 [31]. Significant differences between two groups were determined using the Mann-Whitney U test as described in the Materials and Methods section, respectively.

Acknowledgements

The authors thank members of the Matsumura laboratory for helpful discussion and H. Shindo and M. Shimada for their secretarial support. The authors also thank Dr. Y. Uda (Human Metabolome Technologies, Inc.) for analytical support of metabolomics data. This work was financially supported in part by a Research and Development grant by the New Energy and Industrial Technology Development Organization (NEDO) to Y.M.; the National Cancer Center Research and Development Fund (26-A-14, 29-A-9, 29-S-1 to Y.M. and 26-A-12 to M.Y.; a Project for Cancer Research and Therapeutic Evolution from the Japan Agency for Medical Research and Development (AMED) (17cm0106415h0002) to Y.M.; and JSPS KAKENHI (JP19K16730, JP21K15497) from the Ministry of Education, Culture, Sports, Science and Technology of Japan to T. A.

Data accessibility

Raw sequence data and read count data in this study are available in the DDBJ Sequenced Read Archive under accession numbers DRX224385-DRX224390.

Supplementary materials

Supplementary material associated with this article can be found, in the online version, at doi:10.1016/j.tranon.2021.101186.

References

[1] F. Bray, J. Ferlay, I. Soerjomataram, R.L. Siegel, L.A. Torre, A. Jemal, Global cancer statistics 2018: GLOBOCAN estimates of incidence and mortality worldwide for 36 cancers in 185 countries, CA. Cancer J. Clin. 68 (6) (2018) 394–424, https://doi.org/10.3322/caac.21492, https://doi.org/.

[2] M. Yasunaga, S. Saijou, S. Hanaoka, T. Anzai, R. Tsumura, Y. Matsumura, Significant antitumor effect of an antibody against TMEM180, a new colorectal cancer-specific molecule, Cancer Sci 110 (2) (2019) 761–770, https://doi.org/10.1111/cas.13907, https://doi.org/.

[3] T. Shiraishi, K. Ikeda, Y. Tsukada, Y. Nishizawa, T. Sasaki, M. Ito, M. Kojima, G. Ishii, R. Tsumura, S. Saijou, Y. Koga, M. Yasunaga, Y. Matsumura, High expression of TMEM180, a novel tumour marker, is associated with poor survival in stage III colorectal cancer, BMC Cancer 21 (2021), 302, https://doi.org/10.1186/s12885-021-08046-6 https://doi.org/.

[4] T. Anzai, Y. Matsumura, Topological analysis of TMEM180, a newly identified membrane protein that is highly expressed in colorectal cancer cells, Biochem. Biophys. Res. Commun. 520 (3) (2019) 566–572, https://doi.org/10.1016/j.bbrc.2019.10.070, https://doi.org/.

[5] A. Shevchenko, M. Wilm, O. Vorm, M. Mann, Mass spectrometric sequencing of proteins from silver-stained polyacrylamide gels, Anal. Chem. 68 (5) (1996) 850–858, https://doi.org/10.1021/ac950914h, https://doi.org/.

[6] J. Fernandez, F. Gharahdaghi, S.M. Mische, Routine identification of proteins from sodium dodecyl sulfate- polyacrylamide gel electrophoresis (SDS-PAGE) gels or polyvinyl difluoride membranes using matrix assisted laser desorption/ionization-time of flight- mass spectrometry (MALDI-TOF-MS), Electrophoresis 19 (6) (1998) 1036–1045, https://doi.org/10.1002/elps.1150190619, https://doi.org/.

[7] T. Ooga, H. Sato, A. Nagashima, K. Sasaki, M. Tomita, T. Soga, Y. Ohashi, Metabolomic anatomy of an animal model revealing homeostatic imbalances in dyslipidaemia, Mol. Biosyst. 7 (2011) 1217–1223, https://doi.org/10.1039/c0mb00141d, https://doi.org/.

[8] M.L.B.U.AM Bolger, Trimmomatic, a flexible trimmer for Illumina sequence data, Bioinformatics 30 (15) (2014) 2114–2120, https://doi.org/10.1093/bioinformatics/btu170.

[9] R.D.H Li, Fast and accurate short read alignment with Burrows-Wheeler transform, Bioinformatics 25 (14) (2009) 1754–1760, https://doi.org/10.1093/bioinformatics/btp324.

[10] G.S.W.S.Y Liao, featureCounts: an efficient general purpose program for assigning sequence reads to genomic features, Bioinformatics 30 (7) (2014) 923–930, https://doi.org/10.1093/bioinformatics/btt656.

[11] W. Su, J. Sun, K. Shimizu, K. Kadota, TCC-GUI: A Shiny-based application for differential expression analysis of RNA-Seq count data, BMC Res. Notes. 12 (2019), 133, https://doi.org/10.1186/s13104-019-4179-2 https://doi.org/.

[12] Y. Zhou, B. Zhou, L. Pache, M. Chang, A.H. Khodabakhshi, O. Tanaseichuk, C. Benner, S.K. Chanda, Metascape provides a biologist-oriented resource for the analysis of systems-level datasets, Nat. Commun. 10 (2019), 1523, https://doi.org/10.1038/s41467-019-09234-6 https://doi.org/.

[13] Y. Chen, R. Cairns, I. Papandreou, A. Koong, N.C. Denko, Oxygen consumption can regulate the growth of tumors, a new perspective on the Warburg effect, PLoS One 4 (9) (2009), e7033, https://doi.org/10.1371/journal.pone.0007033 https://doi.org/.

[14] UniProt: a worldwide hub of protein knowledge, Nucleic Acids Res 47 (D1) (2019) D506–D515, https://doi.org/10.1093/nar/gky1049, https://doi.org/.

[15] H. Ji, J. Wang, J. Guo, Y. Li, S. Lian, W. Guo, H. Yang, F. Kong, L. Zhen, L. Guo, Y. Liu, Progress in the biological function of alpha-enolase, Anim. Nutr. 2 (1) (2016) 12–17, https://doi.org/10.1016/j.aninu.2016.02.005, https://doi.org/.

[16] Y. Song, Q. Luo, H. Long, Z. Hu, T. Que, X. Zhang, Z. Li, G. Wang, L. Yi, Z. Liu, W. Y. Fang, S. Qi, Alpha-enolase as a potential cancer prognostic marker promotes cell growth, migration, and invasion in glioma, Mol. Cancer. 13 (2014) 65, https://doi.org/10.1186/1476-4598-13-65, https://doi.org/.

[17] M. Capello, S. Ferri-Borgogno, C. Riganti, M.S. Chattaragada, M. Principe, C. Roux, W. Zhou, E.F. Petricoin, P. Cappello, F. Novelli, Targeting the Warburg effect in cancer cells through ENO1 knockdown rescues oxidative phosphorylation and induces growth arrest, Oncotarget 7 (2016) 5598–5612, https://doi.org/10.18632/oncotarget.6798, https://doi.org/.

[18] A. Fabregat, S. Jupe, L. Matthews, K. Sidiropoulos, M. Gillespie, P. Garapati, R. Haw, B. Jassal, F. Korninger, B. May, M. Milacic, C.D. Roca, K. Rothfels, C. Sevilla, V. Shamovsky, S. Shorser, T. Varusai, G. Viteri, J. Weiser, G. Wu, L. Stein, H. Hermjakob, P. D'Eustachio, The Reactome Pathway Knowledgebase, Nucleic Acids Res 46 (2018) D649–D655, https://doi.org/10.1093/nar/gkx1132, https://doi.org/.

[19] L.M. López-Sánchez, E. Aranda, A. Rodríguez-Ariza, Nitric oxide and tumor metabolic reprogramming, Biochem. Pharmacol. 176 (2020), 113769, https://doi.org/10.1016/j.bcp.2019.113769 https://doi.org/.

[20] A.T. Bender, J.A. Beavo, Cyclic nucleotide phosphodiesterases: Molecular regulation to clinical use, Pharmacol. Rev. 58 (3) (2006) 488–520, https://doi.org/10.1124/pr.58.3.5, https://doi.org/.

[21] M.F. Azevedo, F.R. Faucz, E. Bimpaki, A. Horvath, I. Levy, R.B. De Alexandre, F. Ahmad, V. Manganiello, C.A. Stratakis, Clinical and molecular genetics of the phosphodiesterases (pdes), Endocr. Rev. 35 (2) (2014) 195–233, https://doi.org/10.1210/er.2013-1053, https://doi.org/.

[22] D.S. Chandrashekar, B. Bashel, S.A.H. Balasubramanya, C.J. Creighton, I. Ponce-Rodriguez, B.V.S.K. Chakravarthi, S. Varambally, UALCAN: A Portal for Facilitating Tumor Subgroup Gene Expression and Survival Analyses, Neoplasia (United States) 19 (8) (2017) 649–658, https://doi.org/10.1016/j.neo.2017.05.002, https://doi.org/.

[23] B.J. Altman, Z.E. Stine, C.V. Dang, From Krebs to clinic: glutamine metabolism to cancer therapy, Nat. Rev. Cancer. 16 (2016) 619–634, https://doi.org/10.1038/nrc.2016.71, https://doi.org/.
[24] B.K. Masisi, R. El Ansari, L. Alfarsi, E.A. Rakha, A.R. Green, M.L. Craze, The role of glutaminase in cancer, Histopathology 76 (4) (2020) 498–508, https://doi.org/10.1111/his.14014, https://doi.org/.
[25] F. Huang, Q. Zhang, H. Ma, Q. Lv, T. Zhang, Expression of Glutaminase is up-regulated in colorectal cancer and of clinical significance, Int. J. Clin. Exp. Pathol. 7 (3) (2014) 1093–1100.
[26] S. Saha, S.M. Islam, M. Abdullah-AL-Wadud, S. Islam, F. Ali, K. Park, Multiomics Analysis Reveals that GLS and GLS2 Differentially Modulate the Clinical Outcomes of Cancer, J. Clin. Med. 8 (3) (2019) 355, https://doi.org/10.3390/jcm8030355, https://doi.org/.
[27] D. Yu, X. Shi, G. Meng, J. Chen, C. Yan, Y. Jiang, J. Wei, Y. Ding, Kidney-type Glutaminase (GLS1) is a biomarker for pathologic diagnosis and prognosis of hepatocellular carcinoma, Oncotarget 6 (2015) 7619–7631, https://doi.org/10.18632/oncotarget.3196, https://doi.org/.
[28] M. Szeliga, M. Bogacińska-Karaś, A. Rózycka, W. Hilgier, J. Marquez, J. Albrecht, Silencing of GLS and overexpression of GLS2 genes cooperate in decreasing the proliferation and viability of Glioblastoma cells, Tumor Biol 35 (2014) 1855–1862, https://doi.org/10.1007/s13277-013-1247-4, https://doi.org/.
[29] Z. Tang, B. Kang, C. Li, T. Chen, Z. Zhang, GEPIA2: an enhanced web server for large-scale expression profiling and interactive analysis, Nucleic Acids Res 47 (W1) (2019) W556–W560, https://doi.org/10.1093/nar/gkz430, https://doi.org/.
[30] S. Mei, J. Ke, J. Tian, P. Ying, N. Yang, X. Wang, D. Zou, X. Peng, Y. Yang, Y. Zhu, Y. Gong, R. Zhong, J. Chang, X. Miao, A functional variant in the boundary of a topological association domain is associated with pancreatic cancer risk, Mol. Carcinog. 58 (10) (2019) 1855–1862, https://doi.org/10.1002/mc.23077, https://doi.org/.
[31] Y. Kanda, Investigation of the freely available easy-to-use software 'EZR' for medical statistics, Bone Marrow Transplant 48 (3) (2013) 452–458, https://doi.org/10.1038/bmt.2012.244, 2013 483https://doi.org/.